Integration of Submerged Aquatic Vegetation Motion Within Hydrodynamic Models

Nakayama, K. ; Shintani, T. ; Komai, K. ; Nakagawa, Y. ; Tsai, J. W. ; Sasaki, D. ; Tada, K. ; Moki, H. ; Kuwae, T. ; Watanabe, K. ; Hipsey,…

(Citation)
Water Resources Research,56(8):e2020WR027369-e2020WR027369

(Issue Date)
2020-08

(Resource Type)
journal article

(Version)
Version of Record

AGU ADVANCING EARTH AND SPACE SCIENCE

Water Resources Research

RESEARCH ARTICLE
10.1029/2020WR027369

Key Points:
- A model is presented to capture the changing position of Submerged Aquatic Vegetation blades and validated using laboratory experiments
- Forcing terms that control seagrass movement within a meadow are evaluated
- Estimates of deflected vegetation height and bulk meadow friction coefficients demonstrate the importance of simulating SAV motion

Correspondence to:
K. Nakayama,
nakayama@phoenix.kobe-u.ac.jp

Citation:
Nakayama, K., Shintani, T., Komai, K., Nakagawa, Y., Tsai, J. W., Sasaki, D., et al. (2020). Integration of submerged aquatic vegetation motion within hydrodynamic models. *Water Resources Research*, *56*, e2020WR027369. https://doi.org/10.1029/2020WR027369

Received 19 FEB 2020
Accepted 31 JUL 2020
Accepted article online 3 AUG 2020

Integration of Submerged Aquatic Vegetation Motion Within Hydrodynamic Models

K. Nakayama[1], T. Shintani[2], K. Komai[3], Y. Nakagawa[4], J. W. Tsai[5], D. Sasaki[1], K. Tada[6], H. Moki[7], T. Kuwae[7], K. Watanabe[7], and M. R. Hipsey[8]

[1]Graduate School of Engineering, Kobe University, Kobe, Japan, [2]Faculty of Urban Environmental Sciences, Tokyo Metropolitan University, Hachioji, Japan, [3]Department of Civil and Environmental Engineering, Kitami Institute of Technology, Kitami, Japan, [4]Graduate School of Engineering, Kyushu University, Fukuoka, Japan, [5]Department of Biological Science and Technology, China Medical University, Taichung, Taiwan, [6]Chuden Engineering Consultants, Hiroshima, Japan, [7]Coastal and Estuarine Environment Research Group, Port and Airport Research Institute, Yokosuka, Japan, [8]Aquatic Ecodynamics, School of Agriculture and Environment, The University of Western Australia, Perth, Western Australia, Australia

Abstract Aquatic models used for both freshwater and marine systems frequently need to account for submerged aquatic vegetation (SAV) due to its influence on flow and water quality. Despite its importance, parameterizations are generally adopted that simplify feedbacks from SAV, such as canopy properties (e.g., considering the deflected vegetation height) and the bulk friction coefficient. This study reports the development of a fine-scale non-hydrostatic model that demonstrates the two-way effects of SAV motion interaction with the flow. An object-oriented approach is applied to capture the multiphase phenomena, whereby a leaf-scale SAV model based on a discrete element method is combined with a flow dynamics model to resolve stresses from currents and waves. The model is verified through application to a laboratory-scale seagrass bed. A force balance analysis revealed that leaf elasticity and buoyancy are the most significant components influencing the horizontal and vertical momentum equations, respectively. The sensitivity of canopy-scale bulk friction coefficients to water depth, current speeds, and vegetation density of seagrass was explored. Deeper water was also shown to lead to a smaller decrease in vegetation height. The model approach can contribute to improving assessment of processes influencing water quality, sediment stabilization, carbon sequestration, and SAV restoration, thereby supporting an understanding of how waterways and coasts will respond to changes brought about by development and a changing climate.

Plain Language Summary Aquatic system models that capture aquatic vegetation are increasingly important to help us understand processes controlling carbon budgets (e.g., "blue carbon") and for planning restoration efforts (e.g., Adams et al., 2016, https://doi.org/10.1002/lno.10319). Current models all rely on "static" approaches to account for vegetation via bulk parameterizations, though we know vegetation motion is important (e.g., Abdolahpour et al., 2018, https://doi.org/10.1002/lno.11008). Our study is the first to model the feedback between blade-scale vegetation motion and hydrodynamics to show it is crucial in shaping bottom mixing processes with implications for carbon and nutrient deposition.

1. Introduction

Climate change mitigation and adaptation strategies are urgently needed (IPCC, 2014) to reduce the negative impacts associated with natural disasters, such as flood inundation and landslides (Hirabayashi et al., 2013; Tezuka et al., 2013), biodiversity loss (Dutta et al., 2013; Thuiller, 2007), and land and water degradation (Fragoso et al., 2011; Me et al., 2018; Nakayama et al., 2010, 2013; Sachse et al., 2014; Satoh et al., 2012; Song et al., 2018). Restoration of submerged aquatic vegetation (SAV) in aquatic ecosystems has been suggested as a potential mitigation strategy (Nellemann et al., 2009). For example, while shallow coastal areas have often been assumed to release carbon dioxide to the atmosphere due to inputs of organic matter from rivers (Adiyanti et al., 2016; Cai, 2011), well-vegetated aquatic environments have recently been shown to absorb and capture carbon dioxide—a potential sink of anthropogenic carbon as sedimentary organic carbon, termed "blue carbon" (Duarte et al., 2013). Nellemann et al. (2009) report that coastal blue carbon ecosystems accumulate approximately 55% of the total carbon dioxide captured from the Earth's atmosphere due to photosynthesis. While there is empirical evidence for blue carbon capture in seagrass systems, sequestration rates are highly variable (Lavery et al., 2013; Nakayama et al., 2020), and the conditions that can enhance or disrupt carbon capture and storage remains of topical interest. Similarly in inland waters, SAV has also been revealed to stabilize water quality in rivers (Weitzman et al., 2013), shallow lakes (Hilt et al., 2018), and potentially also within deep lakes (Sachse et al., 2014). A more accurate understanding of the hydrodynamic environment associated with SAV and the various water-vegetation-sediment feedbacks could improve our estimation of carbon storage potential and allow us to devise optimal restoration approaches of SAV in degraded water bodies (e.g., Adams et al., 2018; Prentice et al., 2019).

Given the wide diversity of vegetation forms and hydrologic contexts, numerical models serve an important role to resolve the interaction of SAV with hydrodynamic flows and biogeochemical cycles and to support the management and restoration of SAV communities (Macreadie et al., 2019). To date, the inclusion of SAV within Aquatic Ecosystem Models (AEMs) has focused on either (a) the effect of vegetation on flow hydrodynamics since the vegetation canopy induces drag to the passing flow and affects the water circulation (Weitzman et al., 2015; Zeller et al., 2014) or (b) the role of vegetation in aquatic biogeochemical cycling in the water and sediment (Baird et al., 2016; Trolle et al., 2014). In both cases, the more complex feedbacks between vegetation movement and aquatic system response have yet to be fully accounted for, at least in hydrodynamic-biogeochemical models applied at scales relevant for integrated assessment (Abdolahpour et al., 2018; Adams et al., 2016).

As the vegetation itself can modify the hydrodynamic conditions within a water body (Lacy & Wylie-Echeverria, 2011), depending on plant morphological form and organization of the canopy (e.g., Boothroyd et al., 2016), it must also be acknowledged that individual plants within a meadow may not all behave identically. A number of laboratory studies where the behavior of each shoot and leaf blade has been considered have demonstrated the importance of plant flexibility (Abdolahpour et al., 2018), and, in general, it has been shown that stiff leaves exhibit a higher drag force than more than flexible leaves (Bouma et al., 2005). Mass transport in more flexible canopies has been shown to increase downstream due to enlargement of the exchange zone (Ghisalberti & Nepf, 2009; Murphy et al., 2007). Furthermore, residual currents in the opposite direction to the progressive direction of waves adjacent to the water surface have been found to occur because of the wave setup at the upstream edge of the canopy (Luhar et al., 2010). Interactions between SAV canopy dynamics and flow have historically been evaluated based on the extent of the flow-induced reconfiguration of aquatic vegetation using the Cauchy number (Ca) and the Buoyancy parameter (B) (Luhar & Nepf, 2011, 2016; Nepf, 2012; Whittaker et al., 2015). Ca indicates the relative magnitude of the drag force and elasticity, computed as $\mathrm{Ca} = \rho C_D b U^2 l^3/(2EI)$, where ρ is the density of water, C_D is the drag coefficient, b is the width of blade leaf, U is the horizontal velocity, l is the blade leaf length, E is the elastic modulus, and I is the second moment of inertia. B indicates the relative magnitude of the buoyancy and elasticity, computed as $\mathrm{B} = \Delta\rho g\, b\, t_h\, l^3/(EI)$, where $\Delta\rho$ is the density difference between the water and the blade leaf and t_h is the thickness of blade leaf. These dimensionless parameters have been successfully applied to describe results from field scale case studies (e.g., Luhar & Nepf, 2013).

In parallel, there have been various numerical approaches developed to account for the effect of SAV within hydrodynamic models. The most common has been to apply traditional flow resistance formulae in a hydrodynamic model, such as the use of a bulk friction coefficient (e.g., Manning's roughness). Another has been to develop a coupled hydrodynamic-SAV model under the condition that there is a vegetation "element" per computational horizontal cell (Wilson, 2007; Wilson et al., 2006). In general, the first approach adopts a hydrostatic approximation and is suited to field scale analyses since the horizontal mesh size is coarse and much larger than a vegetation element. For example, Vilas et al. (2017) demonstrated that spatial and temporal patterns of dissolved oxygen concentrations and associated effects on nutrient cycling were able to be adequately captured by including the bulk effect of macrophytes in a three-dimensional shallow lake model. The latter approach provides more detail of the flow-vegetation interaction (Boothroyd et al., 2016; Infantes et al., 2012; Suzuki et al., 2011) and, however, demands finer grid resolution which can considerably increase the computational cost when applying it to environmental systems at larger scales.

To evaluate spatiotemporal variability in vegetation deflection and changes in the canopy bulk friction coefficients under varied hydraulic conditions, a dynamic SAV model can account for the feedbacks between vegetation movement and environmental conditions (Anderson et al., 2006; Busari & Li, 2015; Li

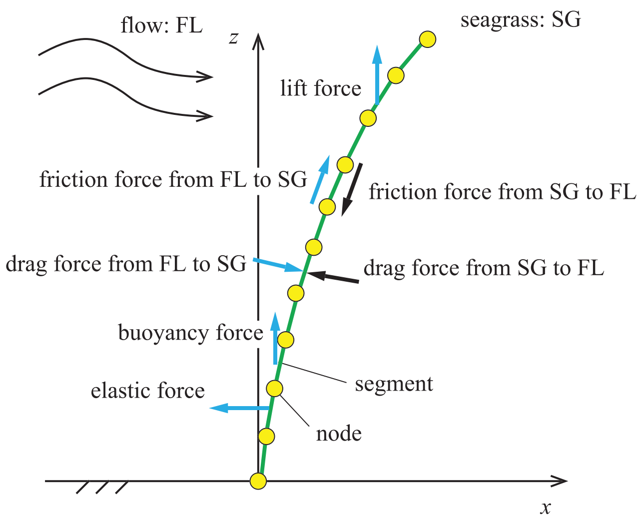

Figure 1. Schematic diagram of SAV model.

et al., 2014; Noarayanan et al., 2012; Stoesser et al., 2003). The development and improvement of methods for integrating individual SAV behavior within hydrodynamic models are required for carbon and nutrient budgeting and restoration decision–making at realistic field scales (Guan & Liang, 2017). At the individual plant scale, there have been several key studies where the movement and position of each leaf blade are modeled by considering the interaction with the current and wave (Abdelrhman, 2007; Dijkstra & Uittenbogaard, 2010; Gac, 2014; Kutija & Hong, 1996; Marjoribanks et al., 2014; Verduin & Backhaus, 2000). In Abdelrhman's (2007) eelgrass model, individual blades were divided into separate segments, each subject to drag force, lift force, friction force, and buoyancy. This approach was found to agree well with laboratory experiments, and the authors successfully reproduced the shelter effect originally noted in Seginer et al. (1976). However, it did not include elastic forces, which Nepf (2012) experimentally demonstrated as one of the most important factors shaping the profile of seagrass (Zhang & Nepf, 2020). Dijkstra and Uittenbogaard (2010) applied a similar method as Abdelrhman (2007) by including the modulus of elasticity with good agreement to laboratory experiments. Marjoribanks et al. (2014) demonstrated an accurate high-resolution hydrodynamic model able to include interactions between flow and river vegetation by accounting for plant rigidity and employing large eddy simulation (LES) to examine turbulence properties in detail. However, open questions remain, theoretical questions related to simulation of flexible vegetation, such as the effect of vegetation density, form and meadow characteristics on vegetation and the flow, and also methodological questions related to model validation, and numerical approaches for addressing scaling and stability issues.

Object-oriented programming methods can enable the effortless combination of multiphase phenomena and the development of integrated environmental modeling (Laniak et al., 2013; Turuncoglu et al., 2013), thereby providing an opportunity to better resolve SAV within AEMs across diverse contexts. As an initial step toward this goal, this study aimed to develop a fully coupled hydrodynamic-SAV model, using an object-oriented programming approach, verified with laboratory experiment data. First, a new individual blade-based SAV model is proposed for seagrass, based on the discrete element method (DEM), considering drag, lift, friction, and elastic forces and buoyancy. A new computational approach for linking the Lagrangian seagrass blade dynamics with the flow fields predicted by a three-dimensional environmental fluid dynamics model (Fantom) is introduced. Second, the coupled Fantom-SAV model is validated by comparing with experimental data on vegetation form during uniform channel flow, and the contribution of each force to vegetation dynamics is investigated under different conditions. Finally, for analyzing field scale phenomenon, velocity, deflected vegetation height, and bulk friction coefficients of seagrass meadows are explored. The approach presented is a necessary step to facilitate simulation of improved flow-vegetation-sediment feedbacks in AEMs and can be used to support scenario modeling of SAV dynamics in aquatic systems.

2. Materials

2.1. SAV Model

Using the DEM approach, each leaf can be divided into connected separate segments, which together are used to compute the Lagrangian blade dynamics. This approach is different from Abdelrhman (2007) and the other model studies reported above who adopt a continuous representation, making it more convenient for combining with a non-hydrostatic hydrodynamic model (Figure 1). The acceleration of the elements is resolved based on the individual force components, including the drag, lift, and friction forces from the flow, the buoyancy of seagrass, and the elastic force associated with leaf stretching. All forces associated with the interaction with the flow are assumed to apply at the node that connects each segment in order to obtain node velocities, and we apply a limiting condition of a constant length of the segment. Since the node velocities of the separate leaf blade segments are solved for using the DEM approach, the SAV model must be combined with a three-dimensional hydrodynamic model via an interface that maps the flow velocity from the hydrodynamic model mesh at the appropriate location, and returning the friction and drag terms to the Navier-Stokes equations accordingly.

In total, the SAV model equation for the horizontal motion of each node is

$$\rho_S V_S \frac{du_S}{dt} = \underbrace{\rho_w \frac{|\mathbf{u}-\mathbf{u_s}|(u-u_S)}{2} C_D A_x}_{\text{drag force}} + \underbrace{\rho_w \frac{|\mathbf{u}-\mathbf{u_s}|(u-u_S)}{2} f_C A_z}_{\text{friction force}} \underbrace{-EIL_S \frac{\partial^4 \zeta_S}{\partial z^4}}_{\text{elastic force}} \tag{1}$$

and for the vertical motion:

$$\rho_S V_S \frac{dw_S}{dt} = \underbrace{\rho_w \frac{|\mathbf{u}-\mathbf{u_s}|(w-w_S)}{2} C_D A_z}_{\text{drag force}} + \underbrace{\rho_w \frac{|\mathbf{u}-\mathbf{u_s}|(w-w_S)}{2} f_C A_x}_{\text{friction force}} + \underbrace{\rho_w \frac{C_L}{2} |\mathbf{u}-\mathbf{u_s}|^2 A_z}_{\text{lift force}} + \underbrace{(\rho_w-\rho_S) g V_B}_{\text{buoyancy}} \tag{2}$$

where t is the time (s), V_S is the volume of a segment (m^3), L_S is the length of a segment (m^3), ρ_S is the density of seagrass (kg m^{-3}), ρ_w is the density of water (kg m^{-3}), $\mathbf{u}$ is the vector of current (m s^{-1}), $\mathbf{u_S}$ is the vector of a node (m s^{-1}), u is the horizontal velocity of the current (m s^{-1}), u_S is the horizontal velocity of a seagrass node (m s^{-1}), C_D is the drag coefficient, A_x is the vertical projected area (m^2), f_C is a friction coefficient, A_z is the horizontal projected area (m^2), E is the elastic modulus (Pa), I is the second moment of inertia (m^4), ζ_S is the displacement of a node (m), w_S is the vertical velocity of a node (m s^{-1}), w is the vertical velocity of the current (m s^{-1}), C_L is the lift force coefficient, g is the acceleration due to gravity (m s^{-2}), and V_B is the buoyancy volume (m^3).

The simulation approach adopted here for elasticity is different from the earlier methods, whereby rigidity is computed as the second derivative of curvature, tempered by a damping factor to manage instability (Marjoribanks et al., 2014). Here, elasticity was captured by approximating the local curvature using backward difference. The speed of SAV nodes is the variable in the fundamental equations of our model based on DEM, although the variable in DEM is the location of an element. Since the fluid is solved by using the fluid velocities, this technique gives computational stability.

2.2. Integration of SAV Model Into the Flow Dynamics Model

The interaction between seagrass and flow is analyzed and evaluated by coupling the SAV model (equations 1 and 2) with the hydrodynamic model Fantom (Nakayama et al., 2014, 2016, 2019). The Fantom code applies the predictor-corrector method to compute the non-hydrostatic effects on flow (Nakayama, 2006; Nakayama & Imberger, 2010; Nakayama et al., 2012) and a generic k-ε length-scale turbulent closure model (Umlauf & Burchard, 2003), which is used with a CA filter (Warner et al., 2005). Drag and friction forces brought about by the leaf blade interaction with the flow field are included in Fantom to take into account the reaction from the leaf to the horizontal and vertical velocity components:

$$M_x = -\rho_w \frac{|\mathbf{u}-\mathbf{u_s}|(u-u_S)}{2}(C_D A_x + f_C A_z) \tag{3}$$

$$M_z = -\rho_w \frac{|\mathbf{u}-\mathbf{u_s}|(w-w_S)}{2}(C_D A_z + f_C A_x) \tag{4}$$

where M_x is the additional horizontal momentum from the leaf blade (N) and M_z is the additional vertical momentum from seagrass (N).

Fantom has been developed based on object-oriented programming, and the initial and boundary conditions and additional source terms are all controlled using the *Lua* language. Parallel computing is available as a byproduct of the object-oriented programming design (Figure 2). In the numerical procedure, the first prediction step is the flow component calculation. In the second step, the predicted flow velocities are used to calculate the moving speed of the leaf nodes based on the DEM. Finally, in the corrector step, the Poisson equation is solved to obtain flow velocities which satisfy the continuity equation, and all values are used in the next step, with a time step of Δt.

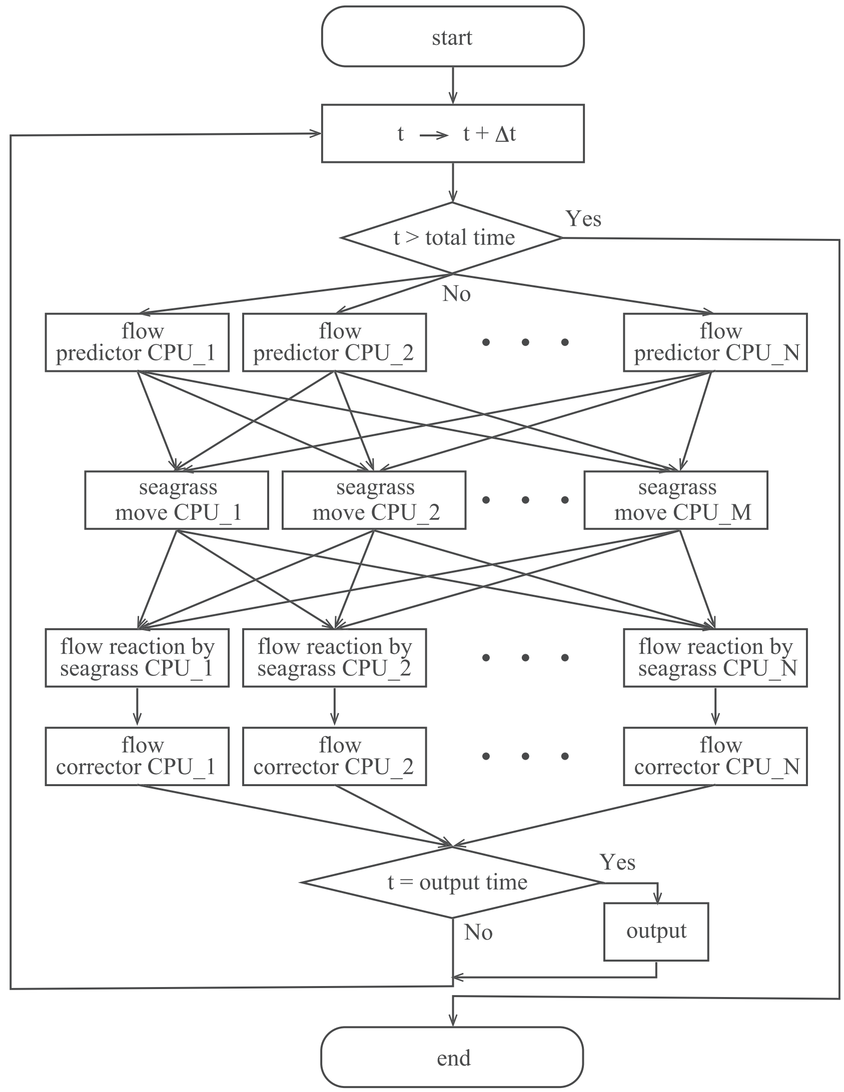

Figure 2. Flow chart of the SAV model. N denotes the number of CPU for wave-current parallel computations, and M means the number of CPU for seagrass (seagrass) parallel computations.

In the second step of the SAV model, seagrass leaf objects find the respective mesh cells that correspond to each node of the leaf adjacent to the bottom and retrieve the flow velocities for the x and z coordinate, u and w. By using Equations 1 and 2, u_S and w_S of the node at the next time step are computed, respectively, and the node locations of the x and z coordinate are updated by using the velocity of the node. We apply a limiting condition of a length of the segment. Then computation of the position of the remaining nodes is done from the second node from the bottom to the tip of the seagrass leaf, for all seagrass blades. After finishing the seagrass leaf motion computation, the mesh cell indices that correspond to all nodes of the leaf objects are identified. Lastly, the flow velocities within the mesh, u and w, are updated accounting for the momentum sink computed using Equations 3 and 4.

2.3. Laboratory Experiment Description

To assess the model, flow in an open channel tank planted with seagrass that was sampled from the Akkeshi-ko estuary in north-eastern Hokkaido, Japan, was used. The seagrass was eelgrass, *Zostera marina*, which was kept refrigerated during transportation to ensure there was little change in the properties of the seagrass before the laboratory experiments. The temperature was less than 10°C during transport, and the seagrass was delivered to the laboratory within 3 days. Four experiments were conducted soon after

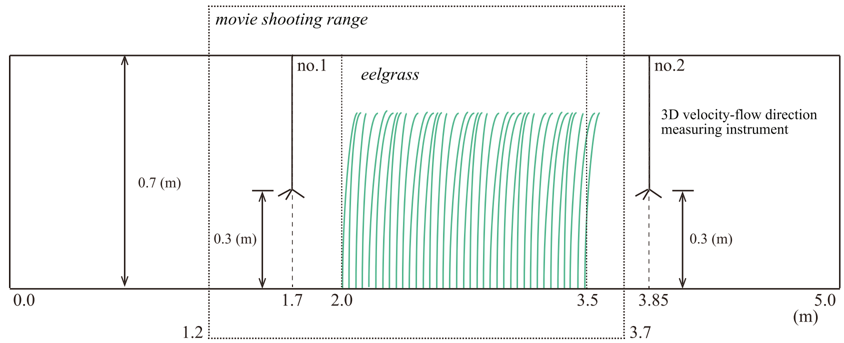

Figure 3. Laboratory experiment setup in an open channel. Velocity was measured at 2 points using an acoustic Doppler current meter. Real seagrass was obtained in the eastern part of Hokkaido Island.

receiving the eelgrass samples. The tank had a water depth of 0.7 m, a width of 0.7 m, and a length of 5.0 m, and unidirectional flow was induced using a pump (Figure 3). The seagrass was deployed over an area within the tank with a length of 1.5 m, as shown in Figure 3. The vegetation density of seagrass was 100 shoots m^{-2}, and each shoot had four leaves with a blade length of 1.0 m for Cases 1 and 2 and with a blade length of 0.35 m for Cases 3 and 4, respectively (Table 1). The average width of a seagrass leaf was 0.010 m, which leaf area of one side was 0.01 m^2 in Cases 1 and 2, for each blade, and 0.0035 m^2 in Cases 3 and 4. The thickness of a seagrass leaf was 0.001 m. The areal leaf biomass was approximately 200 g DW m^{-2} by using the leaf area of both sides of the leaf (m^2) based on sampling *Z. marina* from a vegetated brackish lake (Lake Komuke located in north-eastern Hokkaido near to Akkeshi-ko estuary). A video measurement system was applied to monitor the profile of seagrass, and an acoustic Doppler velocimeter was used to measure velocity at the height of 0.3 m in front of the seagrass (no.1 in Figure 3) and behind the seagrass (no.2 in Figure 3). Two different mean flows of 0.08 and 0.04 m s^{-1} were induced in Cases 1 and 3 and Cases 2 and 4, respectively, to investigate the sensitivity to the unidirectional flow velocity.

2.4. Calibration and Verification of the SAV Model

Several model simulations were configured to reproduce the experimental results. Since unidirectional currents were forced from the left side of the laboratory setup (see Figure 3), similar currents were applied as a boundary condition at the left side of the computational domain in the numerical model. To give the same conditions where there is no wave reflection from the right-side boundary, the length of the computational domain was set to 250 m. Seagrass was located between 32 and 33.5 m from the left-side boundary to give stable unidirectional currents. If we assume that the energy transfers by following the maximum wave speed, it is expected to take about $433/(9.8 \times 0.7)^{0.5} = 165$ s for energy in order to propagate from the left- to right-side boundary and reflect from the right-side boundary to the seagrass. Since the seagrass reached a steady state 40 s, based on the video images after the initial currents commenced, 165 s is considered sufficient to analyze appropriate seagrass motions without the influence of reflection from the right-side boundary. It was confirmed that there was no significant difference in flow fields and seagrass motion across the channel width. Therefore, the vertically resolved two-dimensional computation was applied by giving a width of 0.1 m for the 100 shoots m^{-2} case, with a slip condition on the lateral walls. The width of the computational domain was altered depending on the vegetation density of seagrass. The number of leaves in each shoot was given as four, and the lengths were 1.0 and 0.35 m for Cases 1 to 2 and Cases 3 to 4 (Table 1). Because the computational domain length was 250 m to remove the effect of reflection from the right-side boundary, the horizontal size of the mesh was changed. The minimum horizontal mesh size was 0.05 m around the seagrass which varied from 0.10, 0.20, 0.25, 0.50, and 1.00 m toward the right-side boundary. The vertical mesh size was 0.02 m from the bottom to a height of 0.10 and 0.05 m elsewhere. The time step was 0.0025 s. Initially, we gave no current and no deflection of seagrass. Since we aim to solve the behaviors of seagrasses under shallow

Table 1
Conditions for Laboratory Experiments

Case	Leaf blade length (m)	Uniform current (m s^{-1})
1	1.0	0.08
2	1.0	0.04
3	0.35	0.08
4	0.35	0.04

Note. The condition of flow is uniform, and water depth is 0.7 m.

Table 2
Computational Conditions

Case	EI (N m^2)	E (GPa)	C_D	f_c	Cl
Lab1	1.1×10^{-3} to 4.1×10^{-3}	1.3 to 5.0	1.0	0.30	0.10
E_S	0.8×10^{-3} to 3.1×10^{-3}	1.0 to 3.7	1.0	0.30	0.10
E_L	1.3×10^{-3} to 5.2×10^{-3}	1.6 to 6.2	1.0	0.30	0.10
Cd_S	1.1×10^{-3} to 4.1×10^{-3}	1.3 to 5.0	0.5	0.30	0.10
Cd_L	1.1×10^{-3} to 4.1×10^{-3}	1.3 to 5.0	2.0	0.30	0.10
fc_S	1.1×10^{-3} to 4.1×10^{-3}	1.3 to 5.0	1.0	0.15	0.10
fc_L	1.1×10^{-3} to 4.1×10^{-3}	1.3 to 5.0	1.0	0.60	0.10
Cl_S	1.1×10^{-3} to 4.1×10^{-3}	1.3 to 5.0	1.0	0.30	0.05
Cl_L	1.1×10^{-3} to 4.1×10^{-3}	1.3 to 5.0	1.0	0.30	0.20

Note. Case Lab1 corresponds to Case 1. Capital letters of case names, "E," "Cd," "fc," and "Cl," denote elastic modulus, drag coefficient, friction coefficient, and lift force coefficient. Subscripts, "S" and "L," denote smaller and larger values of "E," "Cd," "fc," and "Cl." The condition of flow is uniform, and water depth is 0.7 m.

water conditions, the vertical diffusion is predominant compared to the horizontal diffusion. Additionally, the aspect ratio between vertical and horizontal grid sizes is small in a real-scale numerical simulation. Therefore, a generic k-ε length-scale turbulent closure model is considered to be more suitable for aquatic plant simulations compared to a LES model which requires high-resolution grids resolving eddies down to the inertial subrange.

We tested several parameter combinations with the SAV model to calibrate the drag, friction, lift force coefficients, and elastic modulus. The drag, lift force, and friction coefficients were set as shown in Case Lab1 of Table 2 (Case 1 in Table 1) by following Abdelrhman (2007). The elastic modulus and buoyancy were determined by trial and error, with Case Lab1 giving the best fit to the laboratory results. Luhar and Nepf (2011) showed the range of elastic modulus of *Z. marina* to be between 0.4 and 2.4 GPa, which is smaller than this study. It may be because their eelgrass length is from 0.3 to 0.5 m and is younger than the eelgrass used in our trials. The profile of seagrass and the velocity in front and behind the seagrass meadows were compared between laboratory experiments and numerical computations for Cases 2 to 4 in Table 1.

2.5. Sensitivity Analysis of SAV Model

To elucidate the contribution of elastic modulus, drag, friction, and lift force coefficients to the seagrass motion and flow behavior, we compared the profile of seagrass leaves and the velocity on either side of the seagrass meadows for Cases Lab1 to Cl_L as in Table 2. For elastic forces, 75% and 125% of the elastic modulus values were applied to Case Lab1 in Cases E_S and E_L, respectively. Similarly, for investigating the contribution of drag, friction, and lift force coefficients, 50% and 150% coefficients were compared to Case Lab1 in Cases Cd_S to Cl_L. It should be noted that different percentages were given in Cases E_S and E_L compared to Cases Cd_S to Cl_L because the contribution of the elastic modulus was more significant relative to the other coefficients, as shown in sections 3.1 and 3.2. Furthermore, the detailed contributions of elastic, drag, friction, and lift forces were quantified for the Lab1 case.

2.6. Field Scale Assessment

Table 3
Computational Conditions for Investigating Velocity, Deflected Vegetation Height, and Friction Coefficient

Case	Water depth (m)	Velocity (m s^{-1})	Density of seagrass (shoots m^{-2})
w05v05d_L	0.5	0.05	100
w05v05d_S	0.5	0.05	44
w05v10d_L	0.5	0.10	100
w05v10d_S	0.5	0.10	44
w10v05d_L	1.0	0.05	100
w10v05d_S	1.0	0.05	44
w10v10d_L	1.0	0.10	100
w10v10d_S	1.0	0.10	44
w15v05d_L	1.5	0.05	100
w15v05d_S	1.5	0.05	44
w15v10d_L	1.5	0.10	100
w15v10d_S	1.5	0.10	44

Note. Seagrass length is 1 m with 600 shoots. "w" and the following number mean water depth, and "v" and the following number mean velocity. For example, "w05v02" means the water depth of 0.5 m and the velocity of 0.5 m s^{-1}. "d" denotes density of seagrass, and subscripts, "S" and "L," denote smaller and larger values of density of seagrass.

To analyze dynamics within a field scale setting, we carried out a simulation setup with a more extensive seagrass meadow. Seagrass was set up in a region with a length of 15 m, which was chosen by using the length scale for the transition when boundary-layer flow changes to mixing-layer-type flow (Ghisalberti & Nepf, 2009). The total length of the computational domain was 250 m, and the horizontal mesh size changed following the same pattern as the laboratory experiment computation cases, from 0.05, 0.10, 0.20, 0.25, 0.50, and 1.00 m. The vertical mesh size was 0.02 m from the bottom to a height of 0.10 and 0.05 m elsewhere. Seagrass was set up from 32 to 47 m from the left-side boundary. The length of the seagrass leaves was set to 1.0 m, with the other conditions the same as the laboratory experiment simulation cases (Case Lab1 of Table 2).

In general, the water depth, unidirectional flow speed, and vegetation density of seagrass shoots can vary considerably in a field situation. Therefore, we explored a total of 12 cases, covering three different water depths, 0.50, 1.0, and 1.5 m, two different unidirectional velocities, 0.05 and 0.10 m s^{-1}, and two different densities of seagrass shoot, 44 and 100 shoots m^{-2}, respectively (Table 3). In the analysis, we calculated the deflected vegetation height as outlined in Luhar and Nepf (2011), flow velocities inside and above the meadow were summarized, and the bulk friction coefficient over the seagrass meadow was estimated.

3. Results

3.1. Model Assessment and Sensitivity

To validate the SAV model performance, we investigated the profile of seagrass in the middle and velocities in front and behind the seagrass meadows for Cases 1 to 4 for unidirectional currents. All coefficients, drag coefficient, friction coefficient, lift force coefficient, and elastic modulus, were determined by applying the SAV model into Case 1 (Case Lab1), and the other cases (Cases 2 to 4) were used to verify the SAV model by using the same coefficients. The profiles showed good agreements with all laboratory experiments (Figure 4). The positions were chosen every 0.2 m from the bottom to the top of seagrass, and $R^2 = 0.99$ for Xb and $R^2 = 0.97$ for Zb, respectively. Also, the horizontal velocities agreed well with the laboratory experiments although the horizontal velocity behind the seagrass meadow was overestimated slightly (Figure 5).

The influence of the elastic modulus, drag coefficient, and friction coefficient on horizontal velocity was investigated (Figure 6). When the elastic modulus decreased in Case E_S compared to Case E_L, the leaves were more bent and a larger volume of free flow conditions was possible above the meadow, resulting in a smaller velocity above the canopy (Figures 6b and 6c). On the other hand, when the drag coefficient increased in Case Cd_L, compared to Case Cd_S, the seagrass blades bent more and smaller horizontal velocities occur inside the meadow (Figures 6d and 6e). Although the same tendency was found when changes to the friction coefficient are made, the sensitivity of the friction coefficient was smaller than the drag coefficient (Figures 6f and 6g).

3.2. Controls on Variability of Seagrass Forces

To quantitatively evaluate the contribution of all forces on seagrass blades, all terms of the SAV model equations were calculated in front, inside, and behind the seagrass meadows for 75 s from the initial conditions (Figure 7). For the horizontal momentum, drag, friction, and elastic forces were considered as follows:

$$M^{*}\mathrm{cd\_h} = \frac{\rho_w}{\rho_S V_S}\frac{|\mathbf{u}-\mathbf{u_s}|(u-u_S)}{2}C_D A_x \tag{5}$$

$$M^{*}\mathrm{fc\_h} = \frac{\rho_w}{\rho_S V_S}\frac{|\mathbf{u}-\mathbf{u_s}|(u-u_S)}{2}f_C A_z \tag{6}$$

$$M^{*}\mathrm{ei\_h} = -\frac{EI}{\rho_S V_S}\frac{\partial^3 w_S}{\partial z^3} \tag{7}$$

Similarly, for the vertical momentum, drag, friction, and lift forces and buoyancy were computed according to

$$M^{*}\mathrm{cd\_v} = \frac{\rho_w}{\rho_S V_S}\frac{|\mathbf{u}-\mathbf{u_s}|(w-w_S)}{2}C_D A_z \tag{8}$$

$$M^{*}\mathrm{fc\_v} = \frac{\rho_w}{\rho_S V_S}\frac{|\mathbf{u}-\mathbf{u_s}|(w-w_S)}{2}f_C A_x \tag{9}$$

$$M^{*}\mathrm{ei\_v} = \frac{\rho_w}{\rho_S V_S}\frac{C_L}{2}|\mathbf{u}-\mathbf{u_s}|^2 A_z \tag{10}$$

$$M^{*}\mathrm{bu\_v} = \frac{\rho_w-\rho_s}{\rho_S V_S} g V_B \tag{11}$$

The maximum drag, friction, and elastic forces were found to appear at the front of the seagrass meadows for horizontal momentum (Figures 7a–7c). The contribution of the friction force was minimal compared to the drag and elastic forces. Since the maximum contribution to seagrass profile is the elastic force, the elastic modulus was found to be one of the most significant coefficients controlling the horizontal momentum.

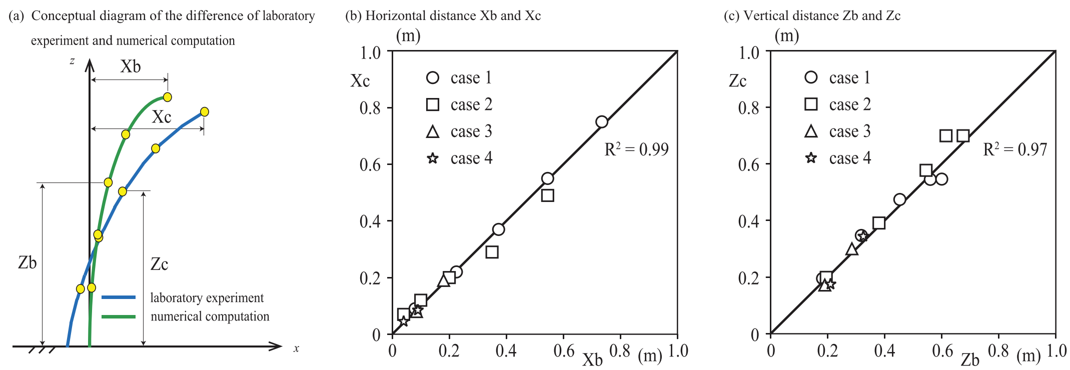

Figure 4. Evaluation of SAV model for four cases, Cases 1 to 4. (a) Definition of positions of every 0.2 m from the root to the top of seagrass. (b) Comparisons of horizontal position between laboratory experiments and numerical computations. (c) Comparisons of vertical position between laboratory experiments and numerical simulations.

For vertical momentum, the most substantial contribution to the seagrass leaf profile was buoyancy, followed by lift forces. The contribution of lift forces to seagrass was almost the same in front, inside, and behind the meadow. The drag force inside the meadow was close to zero, although drag forces in front and behind the meadow had larger values. Friction forces were negligible in the vertical momentum balance.

3.3. Deflected Vegetation Height Prediction at the Field Scale

To investigate the interaction between seagrass meadows and flow at field scales, 15 m meadow of seagrass was set up in a SAV model simulation, with water depth, unidirectional currents, and vegetation density configured as shown in Table 3. Figure 8 is an example of the computational results of Case w15v05d$_L$. Deflected vegetation height was constant in Cases w05v05d$_L$ and w05v05d$_S$ because the leaves reached the water surface (Figure 9). When we pay attention to the same unidirectional current conditions, for example, Case w05v10d$_L$, Case w10v10d$_L$, and Case w15v10d$_L$, the deflected vegetation height was found to increase with an increase in the total water depth because there is more room above the seagrass canopy in larger total water depth. Furthermore, for lower vegetation densities, there was a proportionally larger decrease in the vegetation height. The deflected vegetation height was confirmed to become constant at a distance of 1 to 2 m from the front of the seagrass meadows.

3.4. Velocity Field

Horizontal velocity was investigated inside and above the seagrass meadows. In the shallowest cases, water depth of 0.5 m, horizontal velocity inside (about 0.07 m s^{-1} for Case w05v10d$_L$) and above (about 0.17 m s^{-1} for Case w05v10d$_L$) the seagrass was found to be constant at a distance of 3 m from the front of the meadow. Under the medium water depth case, water depth of 1.0 m, when the unidirectional current speed was 0.05 m s^{-1}, horizontal velocity inside (about 0.05 m s^{-1} for Case w10v10d$_L$) and above (about 0.15 m s^{-1} for Case w10v10d$_L$) the seagrass was constant at a distance of 10 m from the front of the meadow. In the deepest case, water depth of 1.5 m, horizontal velocity inside (about 0.04 m s^{-1} for Case w15v10d$_L$ at the end of seagrass meadows) and above (about 0.14 m s^{-1} for Case w15v10d$_L$ at the end of seagrass meadows) the seagrass did not reach a constant value. Therefore, a constant horizontal velocity inside and above the meadows may occur more quickly when water depths are shallower. Furthermore, even though the currents were the same, deeper water led to smaller horizontal velocities inside the meadow itself.

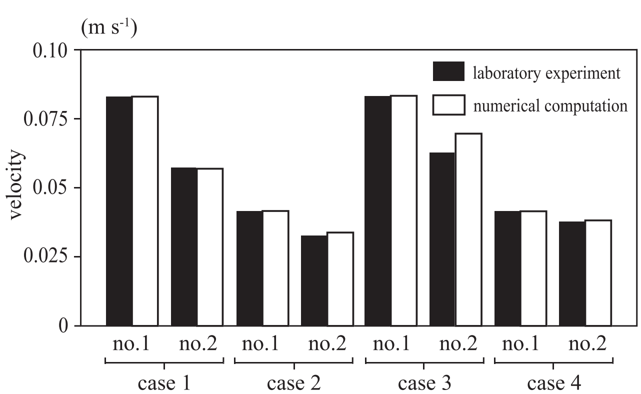

Figure 5. Evaluation of SAV model by using velocities under a uniform current for four cases, Cases 1 to 4. Black and white squares denote laboratory experiments and numerical computations, respectively. "no.1" and "no.2" correspond to the front and behind of seagrass meadow.

3.5. Friction Coefficient Within a Uniform Current

It is useful to evaluate bulk friction coefficients for lakes or coastal systems, where the effects of vegetation need to be parameterized in

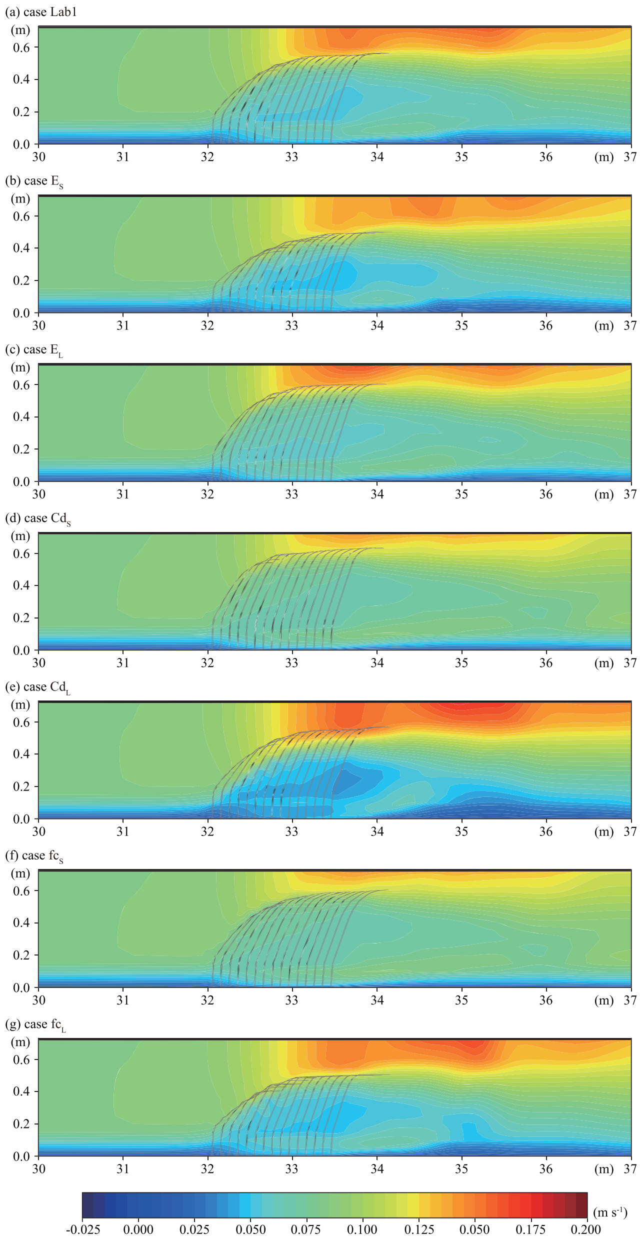

Figure 6. Profiles of seagrass and horizontal velocity. Contours show horizontal velocity. (a) Case Lab1 that corresponds to Case 1. (b) Case E_S. (c) Case E_L. (d) Case Cd_S. (e) Case Cd_L. (f) Case fc_S. (g) Case fc_L.

large-scale models. Therefore, we attempted to estimate the bulk friction coefficients above seagrass meadows using the eddy viscosity and vertical profile of horizontal velocity. For example, the vertical profile of horizontal velocity obtained in Cases w15v05d$_L$ to w15v10d$_S$ is shown in Figures 10d and 10e. The shear stress at the top of seagrass, τ_S (Pa), was obtained using

$$\tau_S = \rho_w K_M \frac{\partial u}{\partial z} \tag{12}$$

where K_M is the eddy viscosity obtained from k-ε model (m^2 s^{-1}). The shear stress can be modeled by introducing friction coefficients above the seagrass meadow, which may yield the bulk friction coefficient as

$$\frac{\tau_S}{\rho_w} = f_S |\boldsymbol{u_w}| u_w \tag{13}$$

$$f_S = \frac{K_M}{|\boldsymbol{u_w}| u_w} \frac{\partial u}{\partial z} \tag{14}$$

where f_S is the bulk friction coefficient and u_w is the depth-averaged horizontal velocity above seagrass (m s^{-1}).

Bulk friction coefficients for a water depth of 0.5 m were obtained around 0.015 at the end of the seagrass meadows for both densities of seagrass, 100 and 44 shoots m^{-2} (Figure 10a). For a water depth of 1.0 m, bulk friction coefficients reached a constant value when unidirectional current speeds were 0.1 m s^{-1}. However, the bulk friction coefficient increased at the end of the seagrass meadows for a unidirectional current speed of 0.05 m s^{-1}. For a water depth of 1.5 m, the bulk friction coefficient reached a constant value when unidirectional current speeds were 0.05 m s^{-1}. For all cases, the bulk friction coefficient increased with decreasing unidirectional current speeds, increasing vegetation density of seagrass, and increasing water depth. In particular, bulk friction coefficients were confirmed to reach 0.047 for Case w15v05d$_L$ with a unidirectional current speed of 0.05 m s^{-1}, vegetation density of 100 shoots m^{-2}, and a water depth of 1.5 m. A bulk friction coefficient of 0.047 is around 20 times that of the smooth bottom friction value of 0.0026.

4. Discussion

The development of a boundary layer around the top of the seagrass meadow was characterized and confirmed using field scale simulations; the lateral variation in the boundary layer would not be accurately captured in models assuming static and rigid seagrass presence. Simulations show that larger water depths lead to a smaller decrease in vegetation height. In previous studies, Ca and B have been applied to estimate deflected vegetation height, and so we made comparisons with the theoretical solutions (Luhar & Nepf, 2011). The leaf blade parameters were set as $l = 1.0$ m, $b = 0.01$ m, $t = 0.001$ m, $\Delta\rho = 0.005$, $C_D = 1.0$, and $EI = 2.3 \times 10^{-3}$ N m^{-2}, and, in the numerical computations, one blade leaf was given with $f_c = 0.30$ and $C_L = 0.10$. For a horizontal velocity of 0.10 m s^{-1}, the theoretical deflected vegetation height is 0.37 m. Since it was shown in this study that water depth influences the deflected vegetation height, three other water depths were compared: 0.5, 1.0, and 1.5 m; these result in the deflected vegetation heights of 0.28, 0.31, and 0.33 m, respectively. As shown in Figure 9, the larger water depth case tends to be similar to the theoretical solution, which provides a reasonable estimate of the deflected vegetation height.

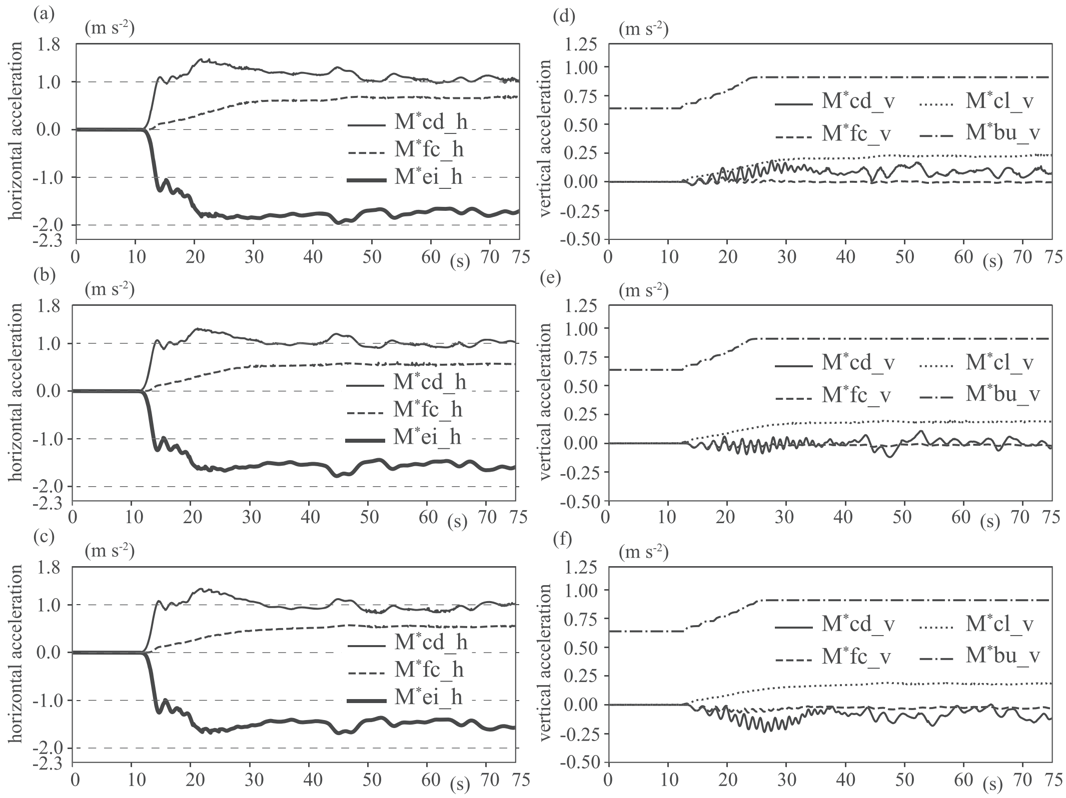

Figure 7. Contribution of elastic modulus, drag, friction, lift forces, and buoyancy to momentum equations obtained from SAV model for Case Lab1. Horizontal acceleration due to drag, friction, and *EI* (a) at the front seagrass, (b) at the middle seagrass, and (c) at the most behind seagrass, respectively. Vertical acceleration due to drag, friction, lift, and buoyancy (d) at the front seagrass, (e) at the middle seagrass, and (f) at the most behind seagrass, respectively.

The adoption of a turbulent closure model also allowed estimation of bulk friction coefficients over seagrass using the vertical profile of horizontal velocity. It showed that bulk friction coefficients increase with increasing water depth, decreasing current speeds, and increasing leaf blade density. The maximum bulk friction coefficient obtained from the dynamic model in this study was 0.047, comparable to Ghisalberti and Nepf (2006) and Luhar et al. (2013) who suggested that 0.05 ($=2f_S$) should be applied in three-dimensional simulations. By looking closer at Case w15v05d$_L$, a typical boundary layer is notable along the top of the seagrass meadow (Figure 8). The integral length scale obtained from the generic length-scale turbulent closure model, l_T, was found to increase from the front of the meadow up to 0.27 m, after which it remains constant until the end, similar to the boundary layer demonstrated in Ghisalberti and Nepf (2009). While LES is increasingly popular in laboratory-scale applications to more

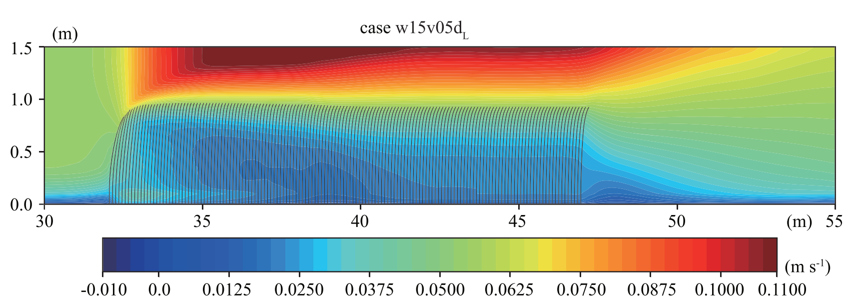

Figure 8. Seagrass and horizontal velocity for Case w15v10d$_L$. Green lines indicate seagrasses from computations. Contours show horizontal velocity.

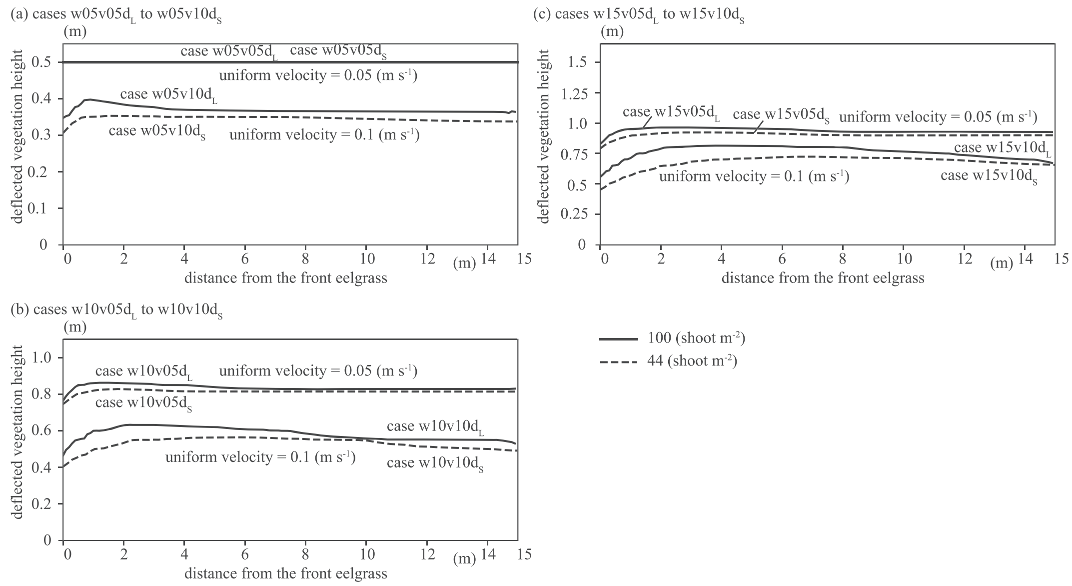

Figure 9. Deflected vegetation height. (a) Cases w05v05d$_L$ to w05v10d$_S$ with the water depth of 0.5 m. (b) Cases w10v05d$_L$ to w10v10d$_S$ with the water depth of 1.0 m. (c) Cases w15v05d$_L$ to w15v10d$_S$ with the water depth of 1.5 m.

accurately compute the interaction between turbulent eddies and vegetation at high resolution (e.g., Marjoribanks et al., 2014), it can be computationally expensive to resolve eddies down to the inertial subrange of the turbulence for field scale problems. Our results give confidence that the use of more simple closure models remains accurate, while also being practical across a wider range of scales. Ultimately, having the flexibility to be able to apply different closure options and model resolutions can support model applicability across a wider range of phenomena from lab to field scales while maintaining a standard coupling interface to the Lagrangian SAV model. Furthermore, the object-oriented programming approach used in

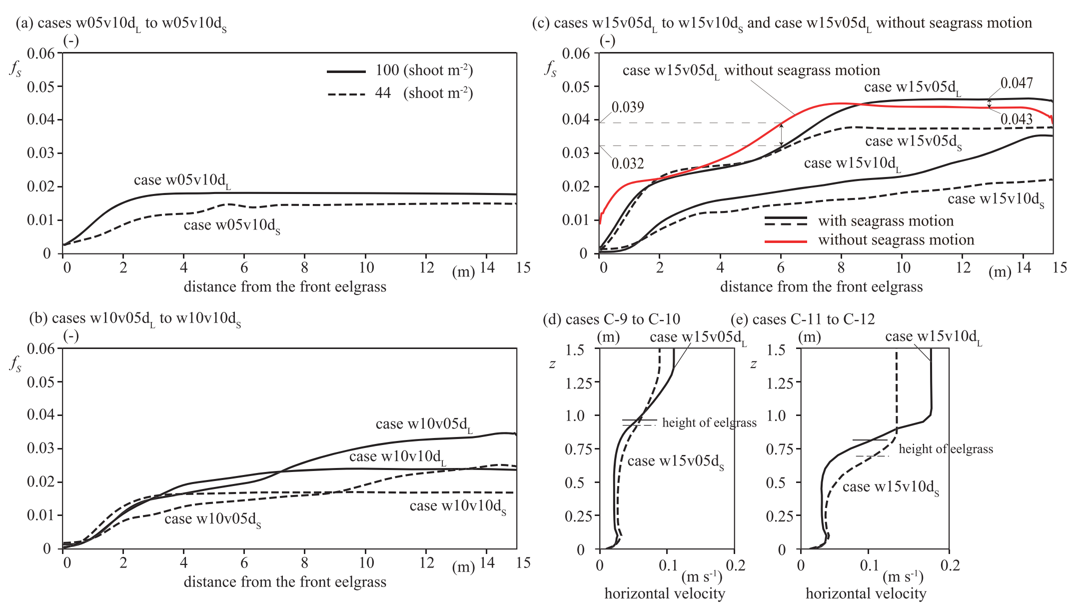

Figure 10. Friction coefficient, (a) Cases w05v10d$_L$ and w05v10d$_S$ with the water depth of 0.5 m, (b) Cases w10v05d$_L$ to w10v10d$_S$ with the water depth of 1.0 m, and (c) Cases w15v05d$_L$ to w15v10d$_S$ with the water depth of 1.5 m and Case w15v05d$_L$ without seagrass motion. Vertical profile of horizontal velocity at the distance of 3 m from the seagrass front, (d) Cases w15v05d$_L$ and w15v05d$_S$ and (e) Cases w15v10d$_L$ and w15v10d$_S$.

10.1029/2020WR027369

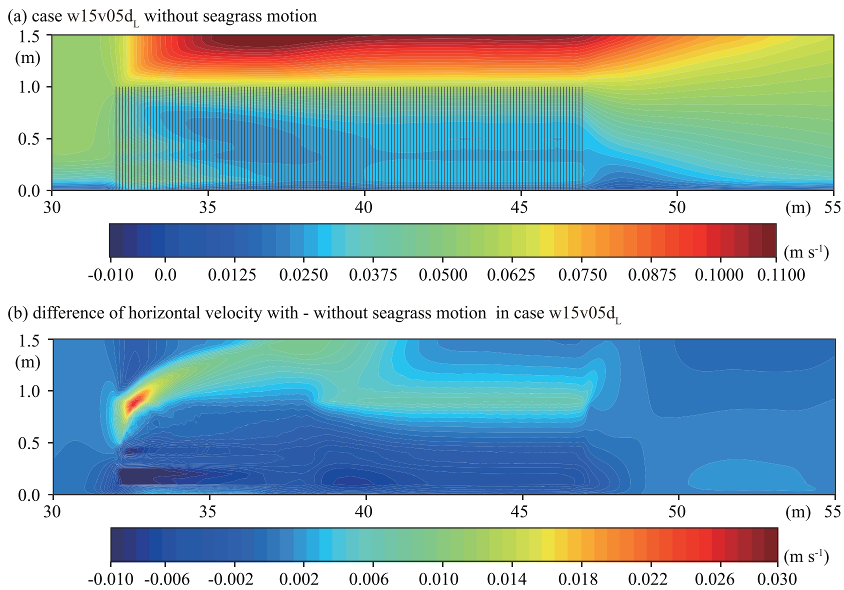

Figure 11. Computation with and without seagrass motion by using Case w15v05d$_L$ conditions. (a) Seagrass and horizontal velocity for Case w15v05d$_L$ without seagrass motion. Contours show horizontal velocity. (b) Difference of horizontal velocity with-without seagrass motion in Case w15v05d$_L$.

the Fantom-SAV model development is useful, in which it can support testing of different computational approaches, closure options, and mesh resolutions.

The focus here has been on the physical interaction of the benthic vegetation with the flow field. The model approach has significant potential for extension to applications associated with the analysis of carbon capture and burial and for improved prediction of nutrient and contaminant fluxes that may impact water quality. For example, when elastic forces are smaller, greater bend in leaf blades causes larger decreases in velocity inside of seagrass meadows, which results in the enhancement of accumulation of particulate organic carbon and nutrients (Duarte et al., 2013). Therefore, if there is no bend in the leaf blades, the rate of carbon and nutrient accumulation rate may decrease. As an example, we compared the Case w15v05d$_L$ condition with a hypothetical no-seagrass-motion equivalent simulation. With no bend in the leaf blades, the friction coefficient 6 m from the meadow front increases from 0.032 to 0.039, about 20% increase (Figure 10). Additionally, flow velocity adjacent to the bottom, which controls resuspension of the bottom sediments, is smaller with seagrass motion than without seagrass motion (Figure 11b). For example, the horizontal velocity at the height of 0.15 m is 0.045 (m s^{-1}) with seagrass motion and increases to 0.057 (m s^{-1}) without seagrass motion, a 27% difference. There are also notable differences in horizontal velocity around the top of the seagrass meadow (Figure 11b). Therefore, if seagrass motion is not included in numerical model simulations, the bulk friction coefficient is underestimated and resuspension from the bottom will be overestimated. In real seagrass meadows, the area of meadow downstream of the edge is notably more extensive than the edge areas, and therefore, it is expected to dominate the amount of vertical flux, friction, and resuspension (Boothroyd et al., 2016; Marjoribanks et al., 2014). Overall, accounting for the bend in the leaf blades is likely to be important for evaluating friction, vertical fluxes, and resuspension around complex meadow geometries in the environment, and further applications of the model could be to explore the feedbacks between water flow regimes, vegetation properties, and sediment dynamics (Adams et al., 2018).

This study has focused on investigating the effect of simple linear seagrass blade morphometries on flow fields, and we developed the SAV model as the first step toward simulations of SAV communities made up of more morphometrically complex and diverse vegetation elements. There are two issues for the application of the SAV model to a real field, one is the necessity of the non-hydrostatic model, and the other is the application of the SAV model into a large-grid numerical simulation. About the first issue, we need to extensively investigate the necessity of the non-hydrostatic model under unidirectional current and wave-current conditions in a real field. Regarding the latter, we may introduce a "super SAV", which can duplicate the interaction with wave and current by integrating thousands of SAV into one super SAV. Since the two issues are closely related, we need to study both problems together for real-scale applications of the SAV model.

Boothroyd et al. (2016) recently highlighted the importance of resolving plant seasonal morphological change on river flow dynamics; however, it has not remained easy to resolve both plant morphological detail and motion to date. Zhang and Nepf (2020) revealed that multiple leaves play a significant role in the sheltering. Through simple extensions of the leaf object model to allow for branching at selected DEM nodes, the approach presented in this study can be further developed for simulating a wider variety of plant forms, thereby allowing simulations that can capture hydrodynamic changes that occur over the full plant life cycle.

5. Conclusion

We have demonstrated that an object-oriented framework can be effectively used to couple a Lagrangian SAV model with a hydrodynamic model to characterize the flexible nature of individual leaves within a meadow, in response to the biophysical environment. The performance of our SAV model was confirmed through the comparisons with laboratory experiments under unidirectional current conditions, showing good agreements in the profiles of leaf blade position and flow velocity. This model result reveals the quantitative influence of drag, friction, and lift forces, buoyancy, and elastic modulus on flow fields around meadows of submerged vegetation. The elastic force is found to be the most influential component in the interaction between horizontal currents and seagrass, whereas buoyancy is revealed to be the most important term in the vertical momentum balance. As with earlier approaches, scaling up the model approach to large-scale environmental systems remains challenging, though applications where the model is applied to evaluate detailed flow fields around SAVs provide opportunities to parameterize reduced models of deflected vegetation height and bulk friction coefficients under various hydraulic conditions. Such approaches can be adopted into large-scale three-dimensional environmental models that adopt a relatively coarse mesh resolution compared to the size of the vegetation elements to allow the essential feedbacks to be captured while maintaining tractability.

Data Availability Statement

The executable binary (windows, Mac, Linux) of the three-dimensional hydrodynamic model, Fantom, used in this study, is available online (from http://www.comp.tmu.ac.jp/shintani/fantom.html). The model outputs are available from https://doi.org/10.5281/zenodo.3930609, "WRR2020: The model outputs for Nakayama et al. (2020)".

Acknowledgments

This work was supported by the Japan Society for the Promotion of Science under Grants 18H01545 and 18KK0119. M. R. H. received funding from LP130100756.

References

Abdelrhman, M. A. (2007). Modeling coupling between eelgrass *Zostera marina* and water flow. *Marine Ecology Progress Series*, *338*, 81–96. https://doi.org/10.3354/meps338081

Abdolahpour, M., Ghisalberti, M., McMahon, K., & Lavery, P. S. (2018). The impact of flexibility on flow, turbulence, and vertical mixing in coastal canopies. *Limnology and Oceanography*, *63*(6), 2777–2792. https://doi.org/10.1002/lno.11008

Adams, P. A., Ghisalberti, M., Lowe, R. J., Callaghan, D. P., Baird, M. E., Infantes, E., & O'Brien, K. R. (2018). Water residence time controls the feedback between seagrass, sediment and light: Implications for restoration. *Advances in Water Resources*, *117*, 14–26. https://doi.org/10.1016/j.advwatres.2018.04.004

Adams, P. A., Hovey, R. K., Hipsey, M. R., Bruce, L. C., Ghisalberti, M., Lowe, R. J., et al. (2016). Feedback between sediment and light for seagrass: Where is it important? *Limnology and Oceanography*, *61*(6), 1937–1955. https://doi.org/10.1002/lno.10319

Adiyanti, S., Eyre, B. D., Maher, D. T., Santos, I., Golsby-Smith, L., Mangion, P., & Hipsey, M. R. (2016). Stable isotopes reduce parameter uncertainty of an estuarine carbon cycling model. *Environmental Modelling & Software*, *79*, 233–255. https://doi.org/10.1016/j.envsoft.2016.02.011

Anderson, B. G., Rutherfurd, I. D., & Western, A. W. (2006). An analysis of the influence of riparian vegetation on the propagation of flood waves. *Environmental Modelling & Software*, *21*(9), 1290–1296. https://doi.org/10.1016/j.envsoft.2005.04.027

Baird, M. E., Adams, M. P., Babcock, R. C., Oubelkheir, K., Mongin, M., Wild-Allen, K. A., et al. (2016). A biophysical representation of seagrass growth for application in a complex shallow-water biogeochemical model. *Ecological Modelling*, *325*, 13–27.

Boothroyd, R. J., Hardy, R. J., Warburton, J., & Marjoribanks, T. I. (2016). The importance of accurately representing submerged vegetation morphology in the numerical prediction of complex river flow. *Earth Surface Processes and Landforms*, *41*(4), 567–576. https://doi.org/10.1002/esp.3871

Bouma, T. J., De Vries, M. B., Low, E., Peralta, G., Tanczos, I. C., & Van de Koppel, J. (2005). Trade-offs related to ecosystem engineering: A case study on stiffness of emerging macrophytes. *Ecology*, *86*(8), 2187–2199. https://doi.org/10.1890/04-1588

Busari, A. O., & Li, C. W. (2015). A hydraulic roughness model for submerged flexible vegetation with uncertainty estimation. *Journal of Hydro-Environment Research*, *9*(2), 268–280. https://doi.org/10.1016/j.jher.2014.06.005

Cai, W. J. (2011). Estuarine and coastal ocean carbon paradox: CO_2 sinks or sites of terrestrial carbon incineration? *Journal of Hydro-Environment Research*, *3*, 123–145.

Dijkstra, J. T., & Uittenbogaard, R. E. (2010). Modeling the interaction between flow and highly flexible aquatic vegetation. *Water Resources Research*, *46*, W12547. https://doi.org/10.1029/2008JB006032

Duarte, C. M., Losada, I. J., Hendriks, I. E., Mazarrasa, I., & Marbà, N. (2013). The role of coastal plant communities for climate change mitigation and adaptation. *Nature Climate Change*, *3*(11), 961–968. https://doi.org/10.1038/nclimate1970

Dutta, D., Write, W., Nakayama, K., & Sugawara, Y. (2013). Design of synthetic impact response functions for flood vulnerability assessment under climate change conditions: Case studies in two selected coastal zones in Australia and Japan. *Natural Hazards Review*, *14*(1), 52–65. https://doi.org/10.1061/(ASCE)NH.1527-6996.0000085

Fragoso, C. R., Marques, D. M. L. M., Ferreira, T. F., Janse, J. H., & Nes, E. H. (2011). Potential effects of climate change and eutrophication on a large subtropical shallow lake. *Environmental Modelling & Software*, *26*(11), 1337–1348. https://doi.org/10.1016/j.envsoft.2011.05.004

Gac, J. (2014). A large eddy based lattice-Boltzmann simulation of velocity distribution in an open channel flow with rigid and flexible vegetation. *Acta Geophysica*, *62*(1), 180–198. https://doi.org/10.2478/s11600-013-0178-1

Ghisalberti, M., & Nepf, H. (2006). The structure of the shear layer in flows over rigid and flexible canopies. *Environmental Fluid Mechanics*, *6*(3), 277–301. https://doi.org/10.1007/s10652-006-0002-4

Ghisalberti, M., & Nepf, H. (2009). Shallow flows over a permeable medium: The hydrodynamics of submerged aquatic canopies. *Transport in Porous Media*, *78*(2), 309–326. https://doi.org/10.1007/s11242-008-9305-x

Guan, M., & Liang, Q. (2017). A two-dimensional hydro-morphological model for river hydraulics and morphology with vegetation. *Environmental Modelling & Software*, *88*, 10–21. https://doi.org/10.1016/j.envsoft.2016.11.008

Hilt, S., Nuñez, A., Marta, M., Bakker, E. S., Blindow, I., Davidson, T. A., et al. (2018). Response of submerged macrophyte communities to external and internal restoration measures in north temperate shallow lakes. *Frontiers in Plant Science*, *9*, 194. https://doi.org/10.3389/fpls.2018.00194

Hirabayashi, Y., Mahendran, R., Kirala, S., Konoshima, L., Yamazaki, D., Watanabe, S., et al. (2013). Global flood risk under climate change. *Nature Climate Change*, *3*(9), 816–821. https://doi.org/10.1038/nclimate1911

Infantes, E., Orfila, A., Simarro, G., Terrados, J., Luhar, M., & Nepf, H. (2012). Effect of a seagrass (*Posidonia oceanica*) meadow on wave propagation. *Marine Ecology Progress Series*, *456*, 63–72. https://doi.org/10.3354/meps09754

IPCC (2014). In Core Writing Team, R. K. Pachauri, & L. A. Meyer (Eds.), *Climate change 2014: Synthesis report. Contribution of Working Groups I, II and III to the Fifth Assessment Report of the Intergovernmental Panel on Climate Change* (p. 151). Geneva, Switzerland: IPCC.

Kutija, V., & Hong, H. T. M. (1996). A numerical model for assessing the additional resistance to flow vegetation. *Journal of Hydraulic Research*, *34*(1), 99–114. https://doi.org/10.1080/00221689609498766

Lacy, J. R., & Wylie-Echeverria, S. (2011). The influence of current speed and vegetation density on flow structure in two macrotidal eelgrass canopies. *Limnology and Oceanography*, *1*, 38–55.

Laniak, G. F., Olchin, G., Goodall, J., Voinov, A., Hill, M., Glynn, P., et al. (2013). Integrated environmental modeling: A vision and roadmap for the future. *Environmental Modelling & Software*, *39*, 3–23. https://doi.org/10.1016/j.envsoft.2012.09.006

Lavery, P. S., Mateo, M., Serrano, O., & Rozaimi, M. (2013). Variability in the carbon storage of seagrass habitats and its implications for global estimates of blue carbon ecosystem service. *PLoS ONE*, *8*(9), e73748. https://doi.org/10.1371/journal.pone.0073748

Li, Y., Wang, Y., Anim, D. O., Tang, C., Du, W., Ni, L., et al. (2014). Flow characteristics in different densities of submerged flexible vegetation from an open-channel flume study of artificial plants. *Geomorphology*, *204*, 314–324. https://doi.org/10.1016/j.geomorph.2013.08.015

Luhar, M., Coutu, S., Infantes, E., Fox, S., & Nepf, H. (2010). Wave-induced velocities inside a model seagrass bed. *Journal of Geophysical Research*, *115*, C12005. https://doi.org/10.1029/2010JC006345

Luhar, M., Infantes, E., Orfila, A., Terrados, J., & Nepf, H. (2013). Field observations of wave-induced streaming through a submerged seagrass (*Posidonia oceanica*) meadow. *Journal of Geophysical Research: Oceans*, *118*, 1955–1968. https://doi.org/10.1002/jgrc.20162

Luhar, M., & Nepf, H. (2011). Flow-induced reconfiguration of buoyant and flexible aquatic vegetation. *Limnology and Oceanography*, *56*(6), 2003–2017. https://doi.org/10.4319/lo.2011.56.6.2003

Luhar, M., & Nepf, H. (2013). From the blade scale to the reach scale: A characterization of aquatic vegetative drag. *Advances in Water Resources*, *51*, 305–316. https://doi.org/10.1016/j.advwatres.2012.02.002

Luhar, M., & Nepf, H. (2016). Wave-induced dynamics of flexible blades. *Journal of Fluids and Structures*, *61*, 20–41. https://doi.org/10.1016/j.jfluidstructs.2015.11.007

Macreadie, P. I., Anton, A., Raven, J. A., Beaumont, N., Connolly, R. M., Friess, D. A., et al. (2019). The future of Blue Carbon science. *Nature Communications*, *10*, 3998.

Marjoribanks, T. I., Hardy, R. J., Lane, S. N., & Parsons, D. R. (2014). High-resolution numerical modelling of flow-vegetation interactions. *Journal of Hydraulic Research*, *52*(6), 775–793. https://doi.org/10.1080/00221686.2014.948502

Me, W., Hamilton, D. P., McBride, C. G., Abell, J. M., & Hicks, B. J. (2018). Modelling hydrology and water quality in a mixed land use catchment and eutrophic lake: Effects of nutrient load reductions and climate change. *Environmental Modelling & Software*, *109*, 114–133. https://doi.org/10.1016/j.envsoft.2018.08.001

Murphy, E., Ghisalberti, M., & Nepf, H. (2007). Model and laboratory study of dispersion in flows with submerged vegetation. *Water Resources Research*, *43*, W05438. https://doi.org/10.1029/2006WR005229

Nakayama, K. (2006). Comparisons of CIP, compact and CIP-CSL2 schemes for reproducing internal solitary waves. *International Journal for Numerical Methods in Fluids*, *51*(2), 197–219. https://doi.org/10.1002/fld.1112

Nakayama, K., & Imberger, J. (2010). Residual circulation due to internal waves shoaling on a slope. *Limnology and Oceanography*, *55*(3), 1009–1023. https://doi.org/10.4319/lo.2010.55.3.1009

Nakayama, K., Komai, K., Tada, K., Lin, H. C., Yajima, H., Yano, S., et al. (2020). Modelling dissolved inorganic carbon considering submerged aquatic vegetation. *Ecological Modelling*, *431*. online

Nakayama, K., Maruya, Y., Nakaegawa, T., Komai, K., Kokubo, K., Ishida, T., & Okada, T. (2013). Projection of "strong wind" events related to recovery from hypoxia in Tokyo Bay, Japan. *Hydrological Processes*, *27*, 3280–3291.

Nakayama, K., Nguyen, H. D., Shintani, T., & Komai, K. (2016). Reversal of secondary circulations in a sharp channel bend. *Coastal Engineering Journal*, *58*, 1650002.

Nakayama, K., Sato, T., Shimizu, K., & Boegman, L. (2019). Classification of internal solitary wave breaking over a slope. *Physical Review Fluids*, *4*(1), 014801. https://doi.org/10.1103/PhysRevFluids.4.014801

Nakayama, K., Shintani, T., Kokubo, K., Kakinuma, T., Maruya, Y., Komai, K., & Okada, T. (2012). Residual current over a uniform slope due to breaking of internal waves in a two-layer system. *Journal of Geophysical Research*, *117*, C10002. https://doi.org/10.1029/2012JC008155

Nakayama, K., Shintani, T., Shimizu, K., Okada, T., Hinata, H., & Komai, K. (2014). Horizontal and residual circulations driven by wind stress curl in Tokyo Bay. *Journal of Geophysical Research: Oceans*, *119*, 1977–1992. https://doi.org/10.1002/2013JC009396

Nakayama, K., Sivapalan, M., Sato, C., & Furukawa, K. (2010). Stochastic characterization of the onset of and recovery from hypoxia in Tokyo Bay, Japan: Derived distribution analysis based on "strong wind" events. *Water Resources Research*, *46*, W12532. https://doi.org/10.1029/2009WR008900

Nellemann, C., Corcoran, E., Duarte, C. M., Valdés, L., De Young, C., Fonseca, L., Grimsditch, G. (2009). Blue carbon. A rapid response assessment. United Nations Environmental Programme. GRID-Arendal. Norway.

Nepf, H. M. (2012). Flow and transport in regions with aquatic vegetation. *Annual Review of Fluid Mechanics*, *44*(1), 123–142. https://doi.org/10.1146/annurev-fluid-120710-101048

Noarayanan, L., Murali, K., & Sundar, V. (2012). Manning's 'n' co-efficient for flexible emergent vegetation in tandem configuration. *Journal of Hydro-Environment Research*, *6*(1), 51–62. https://doi.org/10.1016/j.jher.2011.05.002

Prentice, C., Lewis, M. H., Smith, R. S., & Salomon, A. K. (2019). Reduced water motion enhances organic carbon stocks in temperate eelgrass meadows. *Limnology and Oceanography*, *9999*, 1–16.

Sachse, R., Petzoldt, T., Blumstock, M., Moreira, S., Pätzig, M., Rücker, J., et al. (2014). Extending one-dimensional models for deep lakes to simulate the impact of submerged macrophytes on water quality. *Environmental Modelling & Software*, *61*, 410–423. https://doi.org/10.1016/j.envsoft.2014.05.023

Satoh, C., Nakayama, K., & Furukawa, K. (2012). Contributions of wind and river effects on DO concentration in Tokyo Bay. *Estuarine Coast and Shelf Science*, *109*, 91–97. https://doi.org/10.1016/j.ecss.2012.05.023

Seginer, I., Mulhearn, P. J., Bradely, E. F., & Finnigan, J. J. (1976). Turbulent flow in a model plant canopy. *Boundary-Layer Meteorology*, *10*(4), 423–453. https://doi.org/10.1007/BF00225863

Song, X. P., Hansen, M. C., Stehman, S. V., Potapov, P. V., Tyukavina, A., Vermote, E. F., & Townshend, J. R. (2018). Global land change from 1982 to 2016. *Nature*, 1–5.

Stoesser, T., Wilson, C. A. M. E., Bates, P. D., & Dittrich, A. (2003). Application of a 3D numerical model to a river with vegetated floodplains. *Journal of Hydroinformatics*, *5*(2), 99–112. https://doi.org/10.2166/hydro.2003.0008

Suzuki, T., Zijlema, M., Burger, B., Meijer, M. C., & Narayan, S. (2011). Wave dissipation by vegetation with layer schematization in SWAN. *Coastal Engineering*, *59*, 64–71.

Tezuka, S., Takiguchi, H., Kazama, S., Sarukkalige, R., Sato, A., & Kawagoe, S. (2013). Estimation of the effects of climate change on flood-triggered economic losses in Japan. *Natural Hazards and Earth System Sciences*, *1*, 1619–1649.

Thuiller, W. (2007). Biodiversity: Climate change and the ecologist. *Nature*, *448*(7153), 550–552. https://doi.org/10.1038/448550a

Trolle, D., Elliott, J. A., Mooij, W. M., Janse, J. H., Bolding, K., Hamilton, D. P., & Jeppesen, E. (2014). Advancing projections of phytoplankton responses to climate change through ensemble modelling. *Environmental Modelling & Software*, *61*, 371–379. https://doi.org/10.1016/j.envsoft.2014.01.032

Turuncoglu, U. U., Dalfes, N., Murphy, S., & DeLuca, C. (2013). Toward self-describing and workflow integrated Earth system models: A coupled atmosphere-ocean modeling system application. *Environmental Modelling & Software*, *39*, 247–262. https://doi.org/10.1016/j.envsoft.2012.02.013

Umlauf, L., & Burchard, H. (2003). A generic length-scale equation for geophysical turbulence models. *Journal of Marine Research*, *61*(2), 235–265. https://doi.org/10.1357/002224003322005087

Verduin, J. J., & Backhaus, J. O. (2000). Dynamics of plant-flow interactions for the seagrass *Amphibolis antarctica*: Field observations and model simulations. *Estuarine, Coastal and Shelf Science*, *50*(2), 185–204. https://doi.org/10.1006/ecss.1999.0567

Vilas, M. P., Marti, C. L., Adams, M. P., Oldham, C. E., & Hipsey, M. R. (2017). Invasive macrophytes control the spatial and temporal patterns of temperature and dissolved oxygen in a shallow lake: A proposed feedback mechanism of macrophyte loss. *Frontiers in Plant Science*, *8*, 2097. https://doi.org/10.3389/fpls.2017.02097

Warner, J. C., Sherwood, C. R., Arango, H. G., & Signell, R. P. (2005). Performance of four turbulence closure models implemented using a generic length scale method. *Ocean Modelling*, *8*(1-2), 81–113. https://doi.org/10.1016/j.ocemod.2003.12.003

Weitzman, J. S., Aveni-Deforge, K., Koseff, J. R., & Thomas, F. I. M. (2013). Uptake of issolved inorganic nitrogen by shallow seagrass communities exposed to wave-driven unsteady flow. *Marine Ecology Progress Series*, *475*, 65–83. https://doi.org/10.3354/meps09965

Weitzman, J. S., Zeller, R. B., Thomas, F. I. M., & Koseff, J. R. (2015). The attenuation of current- and wave-driven flow within submerged multispecific vegetative canopies. *Limnology and Oceanography*, *60*(6), 1855–1874. https://doi.org/10.1002/lno.10121

Whittaker, P., Wilson, C. A. M. E., & Aberle, J. (2015). An improved Cauchy number approach for predicting the drag and reconfiguration of flexible vegetation. *Advances in Water Resources*, *83*, 28–35. https://doi.org/10.1016/j.advwatres.2015.05.005

Wilson, C. A. M. E. (2007). Flow resistance models for flexible submerged vegetation. *Journal of Hydrology*, *342*(3-4), 213–222. https://doi.org/10.1016/j.jhydrol.2007.04.022

Wilson, C. A. M. E., Yagci, O., Rauch, H. P., & Olsen, N. R. B. (2006). 3D numerical modelling of a willow vegetated river/floodplain system. *Journal of Hydrology*, *327*(1-2), 13–21. https://doi.org/10.1016/j.jhydrol.2005.11.027

Zeller, R. B., Weitzman, J. S., Abbett, M. E., Zarama, F. J., Fringer, O. B., & Koseff, J. R. (2014). Improved parameterization of seagrass blade dynamics and wave attenuation based on numerical and laboratory experiments. *Limnology and Oceanography*, *59*(1), 251–266. https://doi.org/10.4319/lo.2014.59.1.0251

Zhang, Z., & Nepf, H. (2020). Flow-induced reconfiguration of aquatic plants, including the impact of leaf sheltering. *Limnology and Oceanography*, online, 1–16. https://doi.org/10.1002/lno.11542